Carbon 151 (2019) 120–129

Contents lists available at ScienceDirect

Carbon

journal homepage: www.elsevier.com/locate/carbon

Correlation between the catalytic and electrocatalytic properties of nitrogen-doped carbon nanoonions and the polarity of the carbon surface: Experimental and theoretical investigations

Grzegorz S. Szymański [a], Marek Wiśniewski [a], Piotr Olejnik [b], Stanisław Koter [c], Edison Castro [d], Luis Echegoyen [d], Artur P. Terzyk [a, *], Marta E. Plonska-Brzezinska [e, **]

[a] Faculty of Chemistry, Physicochemistry of Carbon Materials Research Group, Nicolaus Copernicus University in Toruń, Gagarin Street 7, 87-100, Toruń, Poland
[b] Institute of Chemistry, University of Bialystok, Ciolkowskiego 1K, 15-245, Bialystok, Poland
[c] Faculty of Chemistry, Department of Physical Chemistry, Nicolaus Copernicus University in Toruń, Gagarin Street 7, 87-100, Toruń, Poland
[d] Department of Chemistry, University of Texas at El Paso, 500 W. University Ave., El Paso, TX, 79968, USA
[e] Department of Organic Chemistry, Faculty of Pharmacy with the Division of Laboratory Medicine, Medical University of Bialystok, Mickiewicza 2A, 15-222, Bialystok, Poland

ARTICLE INFO

Article history:
Received 18 March 2019
Received in revised form
7 May 2019
Accepted 24 May 2019
Available online 25 May 2019

ABSTRACT

Nitrogen atoms were introduced into carbon nanoonion (CNO) cages by annealing aminated nanodiamonds (AM-NDs) under an inert helium atmosphere and reduced pressure. This procedure provided a convenient tool to control the surface properties, such as polarity, and to make CNOs suitable for various applications. Two series of CNOs were produced using different temperatures (1150, 1450 and 1650 °C) and starting materials, unmodified nanodiamonds (NDs) and AM-NDs. Nitrogen-doped CNOs (NCNOs) were prepared by annealing AM-NDs at 1150 °C via a procedure previously reported by our group. Herein, the surface polarity of the NCNOs and their catalytic and electrocatalytic properties were compared with those of the pristine CNOs obtained from non-functionalized NDs under the same experimental conditions. For these purposes, we used several experimental and theoretical methods, such as X-ray photoelectron spectroscopy, water adsorption-desorption measurements supported by the model proposed by Dubinin and Serpinsky, catalytic tests with a gasometric method and electrochemical studies, including cyclic voltammetry and amperometry. All of the CNOs and NCNOs were evaluated for use as biocompatible mediator-free substrates for horseradish peroxidase in hydrogen peroxide detection.

1. Introduction

Commercially available aminated nanodiamonds (AM-NDs) with crystal sizes between 4 and 6 nm were used for the preparation of nitrogen-doped carbon nanoonions (NCNOs) [1]. The central fullerene at the core of the NCNOs was surrounded by multiple layers of nested concentric graphene shells with increasing diameters. This procedure was a modified version of a procedure proposed previously by Kuznetsov [2–4], where non-modified ND particles were used for the formation of spherical CNOs with an intershell spacing of approximately 0.334 nm, similar to that of highly oriented pyrolytic graphite [5,6]. This procedure produced spherical nanostructures composed of 6–11 layered CNOs. When AM-NDs were used as a starting material, the formation of the carbon nanostructures (CNs) was confirmed by high-resolution transmission electron microscopy (HR-TEM), which indicated that the NCNOs had polyhedral structures rather than spherical structures [1]. The synthesis was carried out at three different temperatures: 1150, 1450 and 1650 °C [1]. At 1150 °C, both samples (unmodified and aminated NDs) showed the formation of inhomogeneous nanoparticles with structures composed of a ND core and outer graphitic layers. Higher temperatures led to the complete transformation of the NDs or AM-NDs into multilayered fullerenes, CNOs and NCNOs, respectively.

* Corresponding author.
** Corresponding author.
E-mail addresses: aterzyk@chem.uni.torun.pl (A.P. Terzyk), marta.plonska-brzezinska@umb.edu.pl (M.E. Plonska-Brzezinska).

https://doi.org/10.1016/j.carbon.2019.05.069
0008-6223/

We report herein a nitrogen-doping approach for the synthesis of CNOs to enhance their enzymatic electrocatalytic properties towards hydrogen peroxide (H_2O_2). It has been observed that N-doping can induce n-type electronic modification, as observed in typical semiconducting materials [7–9]. Nitrogen-doped CNs have been applied as electrocatalysts in oxygen reduction reactions [10–12] as electrochemical sensors and biosensors for H_2O_2 [13–15] and glucose [16], and as the anode material in Li-ion batteries [17]. These nanostructures show better electrochemical performances than non-modified CNs due to the high positive charge density of the carbon atoms adjacent to the nitrogen dopants in the CN structure and the strong electronic affinity of the nitrogen atoms [18].

For H_2O_2 detection, it has been proven that nitrogen doping of CNs increases their electrocatalytic properties [19], biocompatibility [20], hydrophilicity [21] and available surface area for biocatalyst anchoring [22]. However, the electrochemical results have indicated that N-doped CNs produce much higher current densities in comparison to those of pristine CNs [23], and H_2O_2 reduction on both pristine and N-doped CNs proceeds according to the same mechanism [15,24,25]:

$$H_2O_2 + 2e^- + 2H^+ \rightarrow 2H_2O \quad (1)$$

These studies also indicated that before H_2O_2 reduction, physisorption of H_2O_2 ($(H_2O_2)_{ads}$) onto the CN surface occurs [23]. The $(H_2O_2)_{ads}$ receives an electron to produce adsorbed OH ($(OH)_{ads}$), and then $(OH)_{ads}$ receives a second electron to produce H_2O.

Non-enzymatic catalysis of H_2O_2 by CNs has previously been reported by our group and by Chatterjee, for which nitrogen-rich CNOs were used to replace Pt-based catalysts in the oxygen reduction reaction [1,26]. In previous studies, the physicochemical properties of non-modified CNOs and those formed from AM-NDs at different temperatures were discussed in detail [1]. It should be noted that our present findings provide new insights about our reported studies. Herein, we mainly focused on finding the correlation between the polarity of the CNO surface and the catalytic and electrocatalytic properties. Due to the interesting electrocatalytic activity of CNOs and NCNOs in an H_2O_2 environment, we investigated the impact of CNOs on the H_2O_2 reduction process in the presence of the horseradish peroxidase (HRP) enzyme. The prepared enzymatic sensors presented good selectivity, rapid response and high sensitivity due to the biocatalyst immobilization step. Here we showed that CNOs and NCNOs, which were not modified with organic mediators, can be promising biocatalysts to facilitate the direct electron transfer (DET) of enzymatic bioelectrocatalysis.

2. Experimental Section

2.1. Materials and chemicals

All chemicals and solvents used were commercially obtained and used without further purification, which included nanodiamond powder (ND) with crystal sizes between 4 and 6 nm and content greater than 97 wt% (Carbodeon μDiamond® Molto, Vantaa, Finland), urea (≥98%, Sigma-Aldrich, Poland), phosphate buffered saline (PBS, BioPerformance Certified, pH 7.4, Sigma-Aldrich, Poland), *N*-ethyl-*N*′-(3-dimethylaminopropyl)carbodiimide hydrochloride (EDC, ≥98.0%, Sigma-Aldrich, Poland), *N*-hydroxysuccinimide (NHS, ≥98.0%, Sigma-Aldrich, Poland), horseradish peroxidase (HRP, type VI, essentially salt-free, lyophilized powder, Sigma-Aldrich, Poland), anhydrous ethanol (99.8%, Avantor Performance Materials Poland S.A.). All aqueous solutions for electrochemical studies were prepared using deionized water, which was further purified with a Milli-Q system (Millipore).

2.2. Synthetic procedures

Pristine CNOs and NCNOs: Commercially available pristine nanodiamond powder or aminated-nanodiamond (NDs or AMNDs) powder, with crystal sizes between 4 and 6 nm, were used for the preparation of CNOs or NCNOs, respectively. Annealing of the ultradispersed NDs or AMNDs was performed at 1150, 1450 and 1650 °C under a 1.1 MPa He atmosphere with a heating rate of 20 °C min^{-1} (Astro carbonization furnace) [1]. The final temperature was maintained for 1 h, and then the material was slowly cooled to room temperature over a period of 1 h. The furnace was opened, and the CNOs or NCNOs were annealed in air at 400 °C to remove amorphous carbon.

Oxidized CNOs (ox-CNOs): The oxidation reaction of CNOs is based on a modified procedure described by Echegoyen and coworkers in 2006 [27]. An aqueous dispersion of pristine CNOs in deionized water and 3 mol L^{-3} nitric acid were subjected to an ultrasonic bath for 48 h. The solution was poured into 50 mL flasks and repeatedly centrifuged at 6000 rpm for 30 min. After each centrifugation, the aqueous nitric acid was removed with deionized water and ethanol. This process was repeated until complete removal of nitric acid from the aqueous solution was observed (pH = 7). The resulting product was dried in an oven for 8 h at 60 °C to completely evaporate the solvent.

2.3. Enzymatic modification of the working electrode using CNOs or NCNOs

The surface of a glassy carbon electrode (GCE) was polished to obtain a mirror finish using 3.0 μm fine diamond polish and 1.0 μm micropolish alumina (Buehler) on a Texmet/alumina pad (BASi). Afterwards, the GCE was immersed in ethanol, ultrasonicated for several minutes to remove trace amounts of alumina from the electrode surface, rinsed with ethanol and pure water and dried under an Ar atmosphere. The modification of the GCE surface was performed according to our previously reported procedure [28]. First, 2 mg of the active material (CNOs or NCNOs) was dispersed in a solution containing conductive carbon paint and ethanol in a volume ratio of 1:6 and sonicated for 15 min. Subsequently, the surface of the GCE was modified by the drop-coating method. Dispersions of CNOs or NCNOs (10 μL) were added dropwise onto the GCE surface, and the solvent was evaporated under an argon atmosphere. Next, the modified electrode was immersed in an aqueous solution containing 40 mM EDC and 10 mM NHS for 1 h. After this activation step, the GCE/CNO electrode (or GCE/NCNO) was rinsed with MQ water and immersed in a HRP buffered solution. A 10 μL aliquot of the HRP solution (2 mg mL^{-1} in 0.01 M PBS, pH = 7.4) was added onto the GCE/CNO surface (or GCE/NCNO) and allowed to immobilize overnight. After the immobilization step, the modified electrode was rinsed with a buffer solution and MQ water to remove loosely held deposited molecules of the biocatalyst from the GCE surface. HRP immobilization of the GCE/CNO-modified electrode surface was performed at 4 °C in a freezer.

2.4. Electrocatalytic tests

The electrocatalytic studies were performed using a computer-controlled Autolab modular electrochemical system equipped with a PGSTAT 12 potentiostat (Eco Chemie Utrecht, Netherlands) using NOVA 1.7 software (Eco Chemie Utrecht) and a three-electrode cell configuration. The working electrode was a glassy carbon (GC) disk electrode (Bioanalytical System Inc.) with a disk diameter of 2.0 mm. A saturated Ag/AgCl electrode was used as the reference electrode. The counter electrode was made from platinum mesh (0.25 mm). All experiments were performed in water

purified in a Millipore apparatus and saturated with argon.

2.5. Water adsorption-desorption

Water adsorption-desorption measurements were performed at a temperature of 24 °C using a typical gravimetric adsorption apparatus equipped with Baratron pressure transducers (MKS Instruments, Germany). Each sample was desorbed before the measurements at 120 °C under high vacuum until a constant mass was obtained (usually after 3 days).

2.6. Catalytic tests

The rate constants for the heterogeneous decomposition of hydrogen peroxide were measured by a gasometric method [29], [1–3,7]. Typical hydrogen peroxide decomposition experiments were carried out at 20 °C and atmospheric pressure using 26 mg of the catalysts in contact with 25 mL of a 0.385 mol L^{-1} hydrogen peroxide solution. The mixture was stirred with a magnetic rod stirrer, and the reaction was monitored by measuring the volume of O_2 evolved as a function of time. The concentration of H_2O_2 was determined as follows:

$$[H_2O_2] = [H_2O_2]_0 - \frac{2p_{O_2}V_{O_2}}{RTV_{sol}} \quad (2)$$

where $[H_2O_2]_0$ is the initial concentration of H_2O_2, V_{O2} is the volume of evolved O_2 at time t, V_{sol} is the volume of the solution and p_{O2} is the partial pressure of O_2 (atmospheric pressure corrected for the water vapour pressure) [29]. For the H_2O_2 decomposition reaction (disproportionation):

$$2H_2O_2 \rightarrow 2H_2O + O_2 \quad (3)$$

the rate constant, which was calculated directly from the experimental data, was a first-order rate constant k (s^{-1}) defined as [28]:

$$k = -\frac{d[H_2O_2]}{dt} \quad (4)$$

For the decomposition of H_2O_2 on the surface of carbon materials with strongly different specific surface areas and varied amounts of H_2O_2, the apparent reaction constant can be more suitably expressed in the form [2,29]:

$$k_s = \frac{V_{sol}k_{hom}}{m_{cat}S_{BET}} \quad (5)$$

where m_{cat} and S_{BET} are the mass and the specific surface area of the catalyst, respectively. The rate constant k_s (cm s^{-1}) is correlated with the true catalytic activity per unit surface area.

2.7. XPS measurements

The XPS measurements were performed using a multi-chamber UHV analytical system (Prevac, Poland) equipped with a non-monochromatic Al Kα (1486.7 eV) radiation source (VG Scienta SAX 100) and a monochromator (VG Scienta XM 780). The Al Kα source was operated at 12 kV and 30 mA. For all samples, a low-resolution survey scan (0–1200 eV) was performed. The pristine CNO and NCNO powder samples were placed on naturally oxidized Si wafers (ITME, Poland) that had been precoated with approximately 50 nm of Au (purity 99.999%) using molecular beam epitaxy (MBE, PREVAC). The measurements were performed at room temperature. The collected data were fit using CasaXPS software (Casa Software Ltd.).

3. Results and discussion

3.1. X-ray photoelectron spectroscopy studies

Nitrogen atoms were introduced into the CNO structures by annealing aminated nanodiamonds (AM-NDs) under an inert helium atmosphere. The physicochemical properties were systematically discussed for undoped and for the nitrogen-doped CNO samples in Ref. 1. The carbon nanostructures were characterized using transmission (TEM) and scanning electron microscopy, X-ray powder diffractions, Raman and Fourier transform infrared spectroscopy, adsorption/desorption of nitrogen, and differential-thermogravimetric analyses. These results revealed that the structure of undoped and nitrogen-doped CNOs vary with the annealing temperature. TEM results indicated that the nitrogen-doped nanostructures have polyhedral structures rather than spherical.

X-ray photoelectron spectroscopy (XPS) was performed to characterize the amount of each element and their local bonding environment. The survey spectra for the oxidized CNOs (oxCNOs), undoped CNOs and NCNOs obtained at different temperatures (1150, 1450 and 1650 °C) are compared in Figs. SI1-SI3 (see Supplementary Data), and their elemental quantifications are summarized in Table 1. The survey XPS spectra for the AM-NDs and 1150-NCNOs contain three peaks (C 1s, N 1s, and O 1s) and the spectra for the other materials contain two peaks (C 1s and O 1s) (Figs. SI1 and SI2). As has been reported, deconvolution of the high-resolution C 1s spectrum for the undoped CNOs shows a main sp^2 hybridized carbon peak located at 284.5 eV and a minor sp^3 hybridized carbon peak located at 285.1 eV (Table 1) [30,31].

The position of the C 1s peak (at 284.5 eV; graphitic C) varies with the annealing temperature and starting material (unmodified or aminated NDs) (Table 1). It was found that for the NCNO samples obtained at different temperatures, the position of the C 1s peak had shifted to higher binding energies (285.00 eV), in agreement with the results obtained by other authors [33–35]. Additional peaks in the 1150-NCNO spectrum were found at 285.34, 286.09, and 287.50 eV, with the highest intensity being at 286.81 eV. These peaks were tentatively assigned to carbon in sp^2 C=N, sp^3 C-N and/or carbon-oxygen (C-OH, C-O-C, C=O, C-O-C=O, O=C-O) bonds [35]. In our case, the formation of C-O bonds was possible because these peaks were also observed for the 1150-CNO sample, with slight shifts to 285.32, 285.92, 286.50 and 287.16 eV, respectively. During a standard procedure for the formation of CNOs via annealing of NDs, an additional annealing step at 400 °C was performed in air to remove amorphous carbon. This step may also lead to the oxidation of some of the carbon atoms on the outermost CNO layer.

The C 1s spectrum of the oxCNOs could be deconvoluted into seven peaks at 284.74 (main, 58 at.%), 284.13, 285.40 (high, 15.8 at.%), 285.91, 286.52, 287.09, and 289.30 eV, which were assigned to C-C, C-H (main, sp^3 C), C=C (sp^2 C), hydroxyl, ether, carbonyl and carboxyl carbons (Table 1). A slight increase in the full width at half-maximum (FWHM) was observed for the C 1s peak of oxCNOs (2.08 for CNOs and 2.14 for oxCNOs). Larger differences in the FWHM were observed for the C 1s peaks of the materials obtained at lower temperatures, 3.03 for 1150-CNOs and 3.25 for 1150-NCNOs. For all materials, an increase in the FWHM for the C 1s peak was observed, which was attributed to induced disorder in the graphene-based structure [33], and this disorder decreased with increasing annealing temperature during the formation of CNOs from NDs (Table 1).

The ratios of oxygen to other elements for the investigated CNO samples are displayed in Table 1. The O 1s XPS spectra exhibited several binding energy peaks at 531.39, 532.39, 533.51, 530.71 and

Table 1
The dopant contents and elemental distribution of oxCNOs, NCNOs and pristine CNOs as determined from XPS analysis.

Sample	Name	Position (eV)	C [a] (at.%)	Definition
CNOs[b]	C 1s	284.50	100	C-C (sp^2)
		285.10		C-C (sp^3)
oxCNOs	C 1s	284.70	84.7	C-C, C-H (sp^3); C-C (sp^2);
	O 1s	532.70	15.3	C-C; C-OH; C-O-C; C═O; C-O-C═O; O═C-O
				O═C; HO-C; C-O-C
1150-CNOs	C 1s	284.69	89.5	C-C (sp^3); C-C (sp^2);
	O 1s	531.39	10.5	C-C; C-OH; C-O-C; C═O; C-O-C═O; O═C-O
				O═C; HO-C; C-O-C
1450-CNOs	C 1s	284.65	96.5	C-C (sp^3); C-C (sp^2);
	O 1s	533.15	3.5	C-C; C-OH
				O═C; HO-C; C-O-C
1650-CNOs	C 1s	284.67	98.0	C-C (sp^3); C-C (sp^2);
	O 1s	532.67	2.0	C-C; C-OH
				O═C; HO-C;
				C-O-C
AM-NDs	C 1s	284.72	90.8	C-C (sp^3); C-C (sp^2);
	O 1s	531.72	7.5	C-N (sp^3); C-N (sp^2); C-C; C-OH; C-O-C; C═O; C-O-C═O
	N 1s	400.3	1.7	HO-C; C-O-C
				$C\text{-}NH_2$
1150-NCNOs	C 1s	285.00	91.4	C-C (sp^3); C-C (sp^2);
	O 1s	531.00	7.6	C-N (sp^3); C-N (sp^2); C-C;
	N 1s	398.50	1.0	C-OH; C-O-C; C═O; C-O-C═O
				HO-C; C-O-C
				C-N═C (sp^2)
1450-NCNOs	C 1s	285.00	95.8	C-C (sp^3); C-C (sp^2); C-C; C-OH; C-O-C; C═O; C-O-C═O
	O 1s	533.00	4.2	O═C; HO-C;
				C-O-C;
1650-NCNOs	C 1s	285.00	97.4	C-C (sp^3); C-C (sp^2); C-C; C-OH; C-O-C; C═O; C-O-C═O
	O 1s	532.50	2.7	HO-C; C-O-C

[a] C — concentration.
[b] From Ref. [32].

534.72 eV, which varied for the different annealing temperatures. These peaks can be assigned to double-bond oxidized carbon species, single-bond oxidized carbon species, hydroxyl and ether groups bonded to aliphatic or aromatic carbon, oxygen bonded to aromatics and to water adsorbed as a monolayer [36,37]. As expected, the oxygen content decreased with increasing annealing temperature of the NDs or AM-NDs. With increasing annealing temperature (from 1150 to 1650 °C), the oxygen content clearly decreases for both the CNO and NCNO series, from 10.5 ± 0.1 at.% (1150-CNOs) to 2.0 ± 0.1 at.% (1650-CNOs) and from 7.6 ± 0.1 at.% (1150-NCNOs) to 2.7 ± 0.1 at.% (1650-NCNOs) (Table 1).

The XPS data showed that nitrogen substitution only occurred in the CNOs obtained at 1150 °C from AM-NDs (Table 1, Fig. SI3). As shown in Fig. SI3, the N 1s core spectrum for the 1150-NCNOs had a single peak at 398.50 eV, which indicated that the nitrogen atoms had been substituted for the carbon atoms in the sp^2 carbon network (Table 1). This peak is commonly attributed to pyridinic N located at the edge of a graphitic network or bonded to two carbon atoms next to a vacancy [33]. It has also been observed by experimental and theoretical methods [15,23] that pyridinic N shifts the onset potential of H_2O_2 towards more positive values for heterogeneous catalysis and exhibits the best performance for the reduction of the analyte. In the case of AM-ND the N1s peak is located around 400 eV due the presence of amino groups [38].

3.2. Water adsorption-desorption measurements (model calculations)

The adsorption-desorption isotherms are shown in Fig. 1. The data collected in Fig. 1 show that with increasing temperature during the heat treatment of the carbon materials, water adsorption, as well as the hysteresis in the adsorption-desorption isotherms, decreases. To observe the nuances and regularities in Fig. 1, a water adsorption isotherm model was applied to describe the experimental data. For

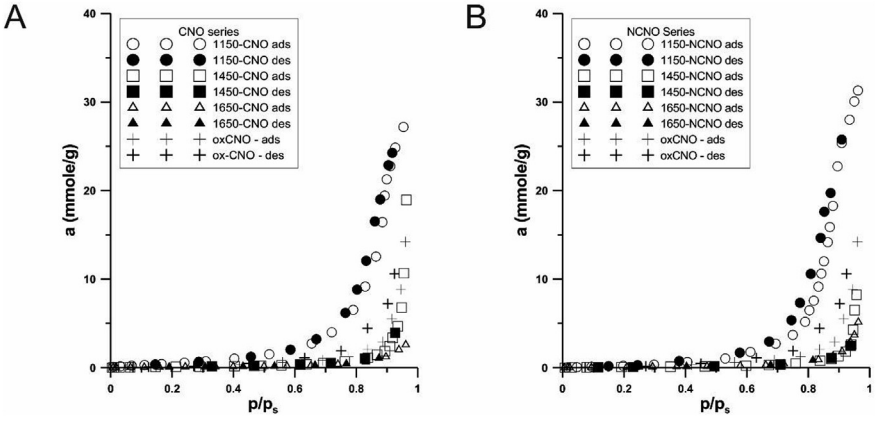

Fig. 1. Water adsorption-desorption isotherms (T = 24 °C) for the (A) CNO and (B) NCNO series.

this purpose, the model proposed by Dubinin and Serpinsky was chosen [39–41], which has been previously labelled the DS2 model [42,43]. The DS2 model is a semi-empirical model modified from the original DS approach. In brief, this model postulates that water adsorption occurs at strongly hydrophilic surface polar sites. At these primary adsorption sites, clusterization occurs, and this process decreases access to the primary centres.

This mechanism leads to the DS2 adsorption isotherm model in the following form:

$$a = c(a_0 + a)(1 - ka)h \tag{6}$$

where a is the adsorption, a_0 is the surface concentration of the primary adsorption sites, h is the relative pressure ($=p/p_s$ where p is the equilibrium and p_s the saturated vapour pressure), c is a ratio of adsorption/desorption constants, and k is a constant corresponding to the loss of primary sites during adsorption.

To characterize the behaviour of the DS2 isotherm equation, we show the results of several model calculations in Fig. 2. An increase in a_0 causes a rapid rise in adsorption (Fig. 2A); an increase in c (Fig. 2B) shifts the adsorption isotherms towards lower pressures, while a decrease in k (Fig. 2C) increases adsorption at intermediate pressures due to lower saturation of the primary adsorption sites. Since Eq. (6) is a quadratic equation with respect to a, there are two solutions for a. We chose the following solution:

$$a = \frac{2a_0ch}{1 - (1 - a_0k)ch + \left(4a_0k(ch)^2 + (1 - (1 - a_0k)ch)^2\right)^{1/2}} \tag{7}$$

To obtain the model parameters (a_0, c and k), Eq. (6) was fit to the experimental data by minimizing the sum of squares of the residuals using the Mathematica® function NonlinearModelFit. Prior to this, the data were analysed using a plot of $a/h = f(a)$. According to Eq. (6), for $ka \ll 1$, the fit should be a straight line. Points that strongly deviated from this line were rejected. The range of the fit was chosen to maximize the value of determination coefficient for linear relationship. This applied especially to points at low pressures, which had the largest experimental errors. A typical example is shown in Fig. SI4 (see Supplementary Data).

The estimated parameters and their standard errors are collected in Table 2. The data collected in Table 2 show that for all studied CNO samples, the value of the a_0 parameter changed dramatically. Since this parameter is strictly related to the number of adsorption sites, one should expect a relation between this value and the polarity of the carbon surface. On the other hand, different authors have noted that the ratio of the XPS-determined O_{1s}/C_{1s} atomic percentages can be successfully applied to indicate the polarity of a carbon surface [44–46].

In fact, the data collected in Fig. 3 confirmed that, for the studied series of CNOs, an exponential correlation between both values exists. To our knowledge, this is the first correlation of this type to be observed for CNOs, specifically, and for carbonaceous materials in general. Due to higher electronegativity of oxygen and its higher content, during the presence of both heteroatoms on carbon surface the role of nitrogen in water adsorption is negligible [47].

3.3. Catalytic tests

CNOs and NCNOs, which are catalytically active toward the H_2O_2 decomposition reaction (disproportionation) (Eq. (2)), were investigated. Kinetic analysis of the H_2O_2 decomposition data suggested that the reaction behaviour follows a pseudo-first-order rate with respect to the H_2O_2 concentration at the beginning of the reaction (Fig. 4), which is similar as that for other carbon materials [48–50].

A decrease in the catalytic activity over time was observed (Fig. 4). This decrease could be caused by deactivation of the most

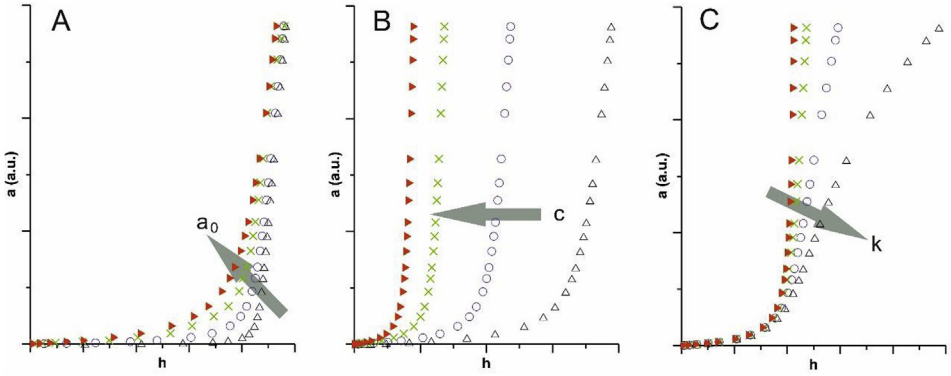

Fig. 2. The influence of the parameters of the DS2 model on the shape of the adsorption isotherms, arrows show the increase in (A) a_0, (B) c and (C) k, respectively. (A colour version of this figure can be viewed online.)

Table 2
Values of the parameters obtained from fitting Eq. (1) to the experimental adsorption data of water and the determination coefficients (R^2) together with the previously published BET surface areas and the XPS-determined ratios of the atomic percentages of the O_{1s}/C_{1s} surface atoms.

Sample	S_{BET} ($m^2\ g^{-1}$)[a]	O_{1s}/C_{1s}	R^2	a_0 ($g\ g^{-1}$)	c	k
oxCNO	448	0.14	0.9985	0.0065 ± 0.0006	1.020 ± 0.007	0.016 ± 0.019
1150-CNO	235	0.11	0.9996	0.0243 ± 0.0007	1.046 ± 0.003	0
1450-CNO	322	0.04	0.9993	0.0030 ± 0.0002	1.033 ± 0.002	0.010 ± 0.003
1650-CNO	454	0.02	0.9985	0.0022 ± 0.0002	1.038 ± 0.014	0.89 ± 0.20
1150-NCNO	255	0.08	0.9998	0.0122 ± 0.0004	1.141 ± 0.004	0.121 ± 0.006
1450-NCNO	296	0.04	0.9915	0.0013 ± 0.0003	1.046 ± 0.007	0.060 ± 0.029
1650-NCNO	383	0.03	0.9998	0.0029 ± 0.00009	1.013 ± 0.003	0.066 ± 0.022

[a] From Ref. [1].

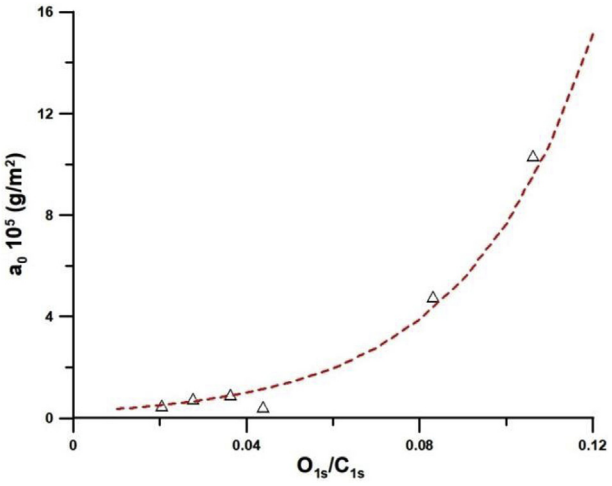

Fig. 3. The correlation between the parameter a_0 of Eq. (1) and the XPS-determined polarity of the CNOs (see Table 1). The dashed line shows the fitting to an exponential function ($R^2 = 0.8999$). (A colour version of this figure can be viewed online.)

active sites [48]. This deactivation was more pronounced for the CNOs. The first-order heterogeneous decomposition rate constants determined from the linear slopes of the ln[H_2O_2] vs. time plots and the volume of the solution, normalized by the BET areas of the CNOs, are displayed in Table 3. The CNO activity was comparable to the activities of other nanocarbons (e.g., carbon nanotubes, graphene oxide), and as with other CNs, the CNOs demonstrated very low activity in comparison to that of macroscale carbons (e.g., activated carbon) [48,49].

For both series (CNOs and NCNOs), the highest catalytic activity was shown by the samples annealed at 1150 °C (1150-CNO and 1150-NCNO). Annealing at higher temperatures resulted in a decrease in the catalytic activity for both series. The samples annealed at 1650 °C demonstrated the lowest activity among all the samples. Additionally, the lowest catalytic activity was shown by the oxCNOs.

It is frequently assumed that the activity of a carbon material results from the presence of electron-rich sites associated with structural defects and edge graphene planes or the presence of heteroatoms (e.g., O or N) [50–56]. According to the XPS measurements (Table 1), annealing resulted in the removal of heteroatoms (mainly oxygen) from the CNOs. The higher the annealing temperature was, the lower the heteroatom content and the lower the catalytic activity. There was a positive correlation between the rate constant and the contents of the C-O- and C-O-C moieties in the CNOs. A similar correlation has been observed for H_2O_2 decomposition over activated carbons [52,55].

It is well known that the presence of oxygen and nitrogen heteroatoms (e.g., O and N) in a carbon matrix influences its activity toward the decomposition of H_2O_2 by altering the electronic properties of the carbon [53,54]. The presence of basic oxygen and/or nitrogen-containing surface species enhances the catalytic activity [48–55]. The presence of C-O- and C-O-C moieties in the CNOs could be attributed to the presence of basic surface functionalities such as chromene-like and pyrone-like structures, which are catalytically active in H_2O_2 decomposition [52,55]. The lowest catalytic activity being observed for the oxCNOs, despite their having the highest oxygen content, most likely resulted from the presence of acidic groups that can inhibit the catalytic activity [48–55].

It has been suggested that the H_2O_2 decomposition occurs via free radical ($OH^{\cdot}$/$OOH^{\bullet}$) intermediates, whose formation would take place through an electron-transfer reaction similar to the Fenton mechanism, with AC and AC^{+} as the reduced and oxidized catalyst states [45,47–49,52,53]:

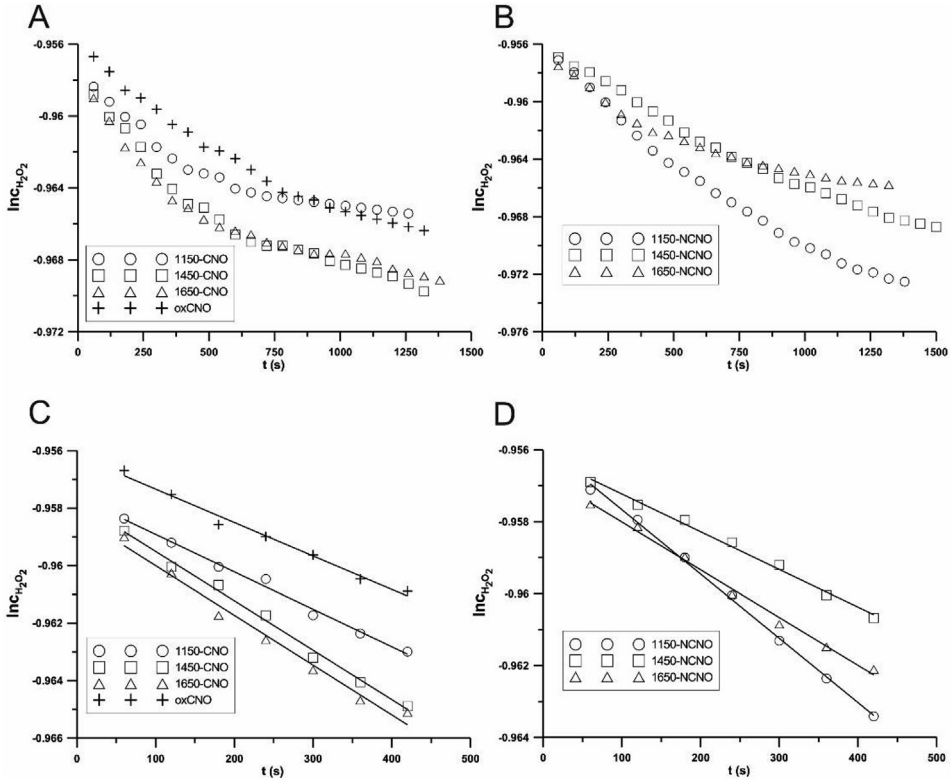

Fig. 4. Kinetic plots of H_2O_2 decomposition investigated over oxCNO (+), CNOs (A, C) and NCNOs (B, D). The CNOs or NCNOs were prepared at different temperatures: (○) 1150 °C; (□) 1450 °C and (△) 1650 °C.

Table 3
The values of apparent rate constants k and k_s for the H_2O_2 decomposition reaction in the presence of CNOs and NCNOs.

Catalyst	$k^a 10^5$ (s^{-1})	R^2	$k_s{}^a 10^9$ (cm s^{-1})	O1s/C1s	C-O-H[a] (at.%)	C-O-C[a] (at.%)
oxCNO	1.09	0.9874	2.18	0.14	6.9	3.2
1150-CNO	1.29	0.9915	4.98	0.11	17.3	20.3
1450-CNO	1.73	0.9933	4.89	0.04	9.4	6.7
1650-CNO	1.69	0.9839	3.45	0.02	8.6	4.5
1150-NCNO	1.73	0.9980	6.62	0.08	18.3	23.0
1450-NCNO	1.10	0.9932	3.49	0.04	10.0	6.2
1650-NCNO	1.44	0.9939	3.42	0.03	6.3	3.6

[a] Amount of carbon as C-O-H or C-O-C moieties, calculated from deconvoluted XP C1s spectra. (% Area × total carbon content (at%)/100%).

$$AC + H_2O_2 \rightarrow AC^+ + OH^- + OH^\bullet \quad (8)$$

$$AC^+ + H_2O_2 \rightarrow AC + H^+ + OOH^\bullet \quad (9)$$

The recombination of free radical species (OH^-/$OOH^\bullet$) in the liquid phase and/or onto the activated carbon surface will produce water and oxygen according to reactions (9) and (10), respectively:

$$OH^\bullet + OOH^\bullet \rightarrow H_2O + O_2 \quad (10)$$

$$OH^\bullet AC^+ + OOH^\bullet AC \rightarrow H_2O + O_2 + AC^+ + AC \quad (11)$$

being the overall reaction, according to this mechanism:

$$2H_2O_2 \rightarrow 2H_2O + O_2 \quad (12)$$

There are reports on a correlation between carbon basic sites and its reduction sites [48] as well as hydroxyl radical generation yield [55,56]. In the report [55] was shown that hydrogen peroxide decomposes via $^\bullet$OH formation, mainly through the interaction with active surface sites of carbon in the form of basic functional groups like chromene groups.

In addition, carbon basic sites may facilitate H_2O_2 decomposition due to deprotonation of H_2O_2 to HOO^-. The HOO^- anion is less stable than the H_2O_2 itself, and decomposes very readily [48,49].

3.4. Electrocatalytic properties of the NCNOs in enzymatic sensing systems

To evaluate the electrochemical enzymatic catalytic performance of the CNOs and NCNOs, cyclic voltammetry (CV) and amperometry studies were performed. To obtain a novel biosensor for the enzymatic detection of hydrogen peroxide (H_2O_2), a glassy carbon electrode (GCE) was modified with NCNOs (GCE/NCNOs) or pristine CNOs (GCE/CNOs) for comparison. In this study, the CNOs and NCNOs were investigated for use as a platform for horseradish peroxidase (HRP) immobilization and the subsequent enzymatic catalytic detection of H_2O_2. H_2O_2 combines with HRP enzyme to form a HRP compound, followed by the reduction of this compound to the original HRP enzyme [57]:

$$HRP\ (Red) + 2H_2O_2 \rightarrow HRP\ compound\ (Ox) + 2H_2O \quad (13)$$

$$HRP\ compound\ (Ox) + 2e^- + 2H^+ \rightarrow HRP\ (Red) + H_2O \quad (14)$$

The potential application of GCE/NCNOs or GCE/CNOs was investigated in a three-electrode cell (working electrode: GCE, reference electrode: Ag/AgCl and counter electrode: Pt) using CV and amperometry, following modification of the GCE, the procedure is described in the Experimental Section. Figs. 5 and 6 show the CV voltammograms of the GCE/CNOs and GCE/NCNOs (CNs were obtained at

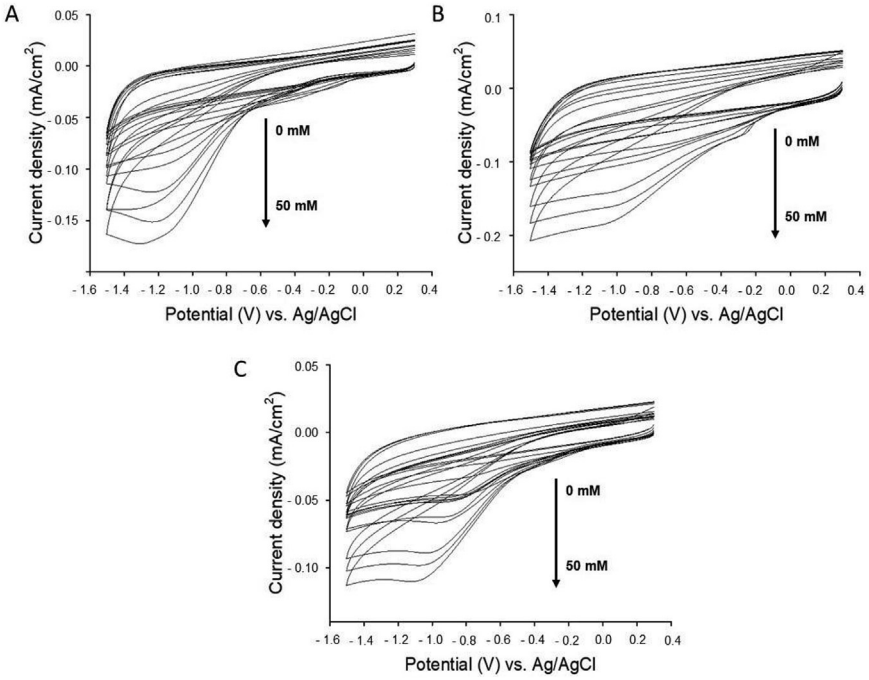

Fig. 5. CVs for the GCE/CNOs with HRP, with CNOs prepared at different temperatures: (A) 1150 °C, (B) 1450 °C and (C) 1650 °C, in the absence and presence of H_2O_2 (from 0 to 50 mM) in 0.01 M phosphate buffered saline (pH = 7.4) at a scan rate of 10 mV s^{-1}.

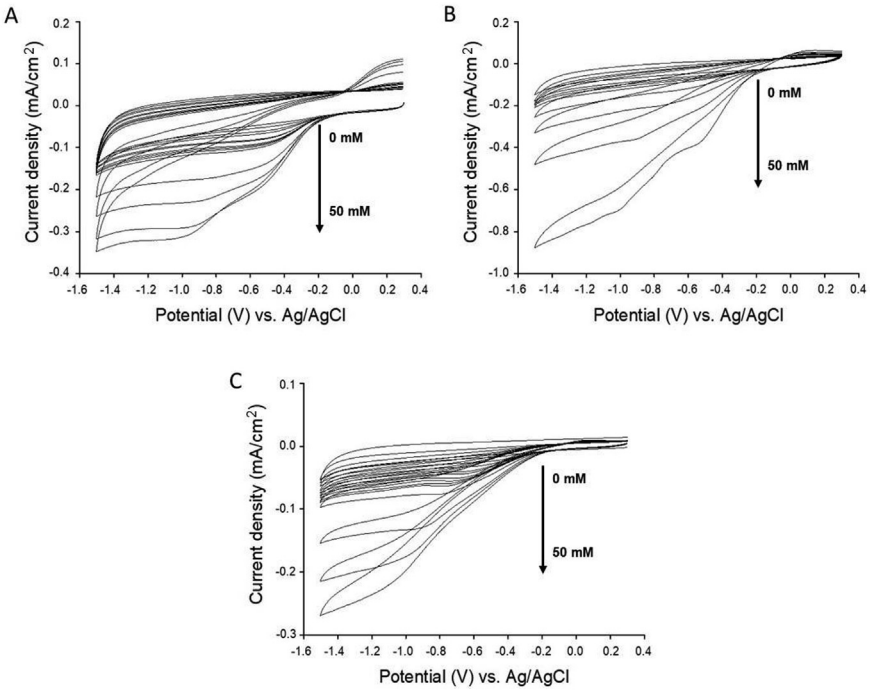

Fig. 6. CVs for the GCE/NCNOs with HRP, with NCNOs prepared at different temperatures: (A) 1150 °C, (B) 1450 °C and (C) 1650 °C, in the absence and presence of H_2O_2 (from 0 to 50 mM) in 0.01 M phosphate buffered saline (pH = 7.4) at a scan rate of 10 mV s^{-1}.

different temperatures: 1150, 1450 and 1650 °C), respectively, in the absence and presence of H_2O_2 (from 0 to 50 mM) in phosphate buffered saline (PBS, pH = 7.4) at a scan rate of 10 mV s^{-1} over a potential window ranging from 400 to −1500 mV vs. Ag/AgCl. The subsequent addition of H_2O_2 to the solution caused an exceptional increase in the reduction current of the analyte for both the CNO and NCNO series (Figs. 5 and 6). This behaviour proved that all tested GCE/CNO and GCE/NCNO electrodes with immobilized HRP had significant activity towards H_2O_2 bioelectrocatalytic reduction (Eq. (8) and (9)). This means that all the modified electrodes had a uniform morphology and a conductive character that created an appropriate intermediary layer for HRP immobilization. Additionally, HRP shifted the H_2O_2 electroreduction potential to more positive values, which was facilitated by a direct electron transfer (DET) mechanism [58]. Here, we also found that the incorporation of HRP into the electrocatalytic systems led to an increase in the H_2O_2 reduction current [1].

By comparing the results of Figs. 5 and 6, the system composed of HRP and NCNOs was capable of driving H_2O_2 reduction much more efficiently (e.g., at more positive potentials and at higher current densities) in comparison to the analogous systems containing CNOs. Importantly, the electrochemical studies showed that the 1450-NCNOs exhibited higher electrocatalytic activity towards H_2O_2 than the other two samples obtained from AM-NDs (1150-NCNOs and 1650-NCNOs, Fig. 7).

Fig. 7 shows the relation between the current density and the reduction of H_2O_2 at different analyte concentrations using GCE/CNOs (Fig. 7A) and GCE/NCNOs (Fig. 7B). Fig. 7 confirmed the stable and reproducible current responses for all CNO and NCNO materials. The recorded current increased with increasing analyte concentration for both series of carbon electrodes. The dependence of the reduction peak current on the concentration of H_2O_2 for both electrode series was found to be linear within the tested analyte concentration range of 1–50 mM. The slopes of the calibration curves indicated a significant difference in the sensitivity toward the H_2O_2 concentration between the GCE/CNO and GCE/NCNO electrodes with immobilized HRP. The sensitivities of these enzymatic electrodes were 20.828 and 7.407 μA/mM cm^2 for GCE/NCNO and GCE/CNO electrodes, respectively. Compared to the performance of previously reported enzymatic H_2O_2 sensors, the modified electrodes investigated in this study displayed very good comprehensive performances (Table SI1).

Amperometry provides important information about the electrocatalytic activity and the stability of the tested biosensing systems

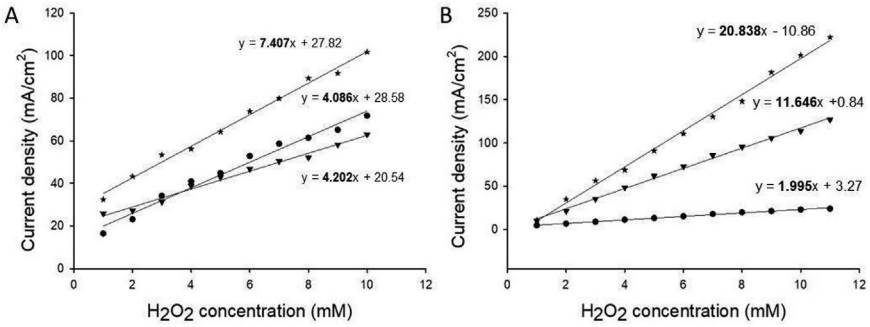

Fig. 7. Calibration curves of the current densities and H_2O_2 concentrations on (A) GCE/CNO and (B) GCE/NCNO electrodes with immobilized HRP in 0.01 M PBS (pH = 7.4). The CNOs and NCNOs were obtained at different temperatures: (•) 1150 °C, (★) 1450 °C and (▼) 1650 °C. Operating potential: -0.5 V.

(Fig. SI5). The applied potential of −500 mV vs. Ag/AgCl is very close to the formal reduction potential ($E^{\circ\prime} = -467$ mV) of the Fe(III)/Fe(II) redox couple at a pH of approximately 7 [59]. The reduction current of H_2O_2 was proportional to the concentration of the analyte and related to the activity of the HRP enzyme [60]. The HRP-functionalized GC/NCNO electrodes exhibited sensitive and rapid current responses upon subsequent additions of H_2O_2 with increasing concentration of the analyte. All of the modified GCEs (NCNOs obtained at different temperatures) revealed constant behaviour during the amperometric measurements over 600 s. The time between subsequent stable current responses was less than 4 s, which proved that rapid electron transfer between the HRP active site and the electrode surface took place. This was due to the large active surface area created by the uniformly loaded NCNO film on the GCE electrode.

There were several factors that affected the electrocatalytic properties of the CNOs and NCNOs. First, there was a positive correlation between electrocatalytic activity and NCNO hydrophobicity. The electrocatalytic current increased with increasing NCNO hydrophobicity. A similar effect has been observed for other CN materials with low oxygen contents [61,62]. The excellent properties of these CN–enzyme conjugates were attributed to the hydrophobic interactions between the enzymes and the CNs [61,62]. The highest electrocatalytic activity was observed for the 1450-NCNOs, which may have resulted from its higher electrical conductivity [63,64], as well as the higher activity of its immobilized HRP compared to the activity of HRP immobilized on the other samples.

4. Conclusions

In summary, we developed a family of nanostructured carbon catalysts by using AM-ND particles for the formation of NCNOs. Several experimental and theoretical methods were performed to identify the correlations between the physicochemical properties and catalytic/electrocatalytic performance of the CNOs and NCNOs.

CNOs and NCNOs adsorbed water following to the mechanism of the DS2 model. With increasing thermal treatment, the number of active sites decreased which correlated well with the XPS-determined O_{1s}/C_{1s} atomic ratios. Removal of the active sites by thermal treatment reduced the degree of adsorption-desorption hysteresis. The higher the temperature of treatment was the lower the catalytic activity. In comparison to activated carbons, the CNOs demonstrated lower catalytic activity.

A system composed of HRP and NCNOs was capable of driving H_2O_2 reduction much more efficiently than analogous systems containing CNOs. Importantly, the electrochemical studies showed that the 1450-NCNOs exhibited the highest electrocatalytic activity towards H_2O_2. The catalytic and electrocatalytic performances of the NCNOs were strongly associated with their mesoporous structure, homogenous distributions of defects and active nitrogen sites, hydrophobicity and homogenous distribution of HRP on the carbon matrix. NCNOs were active toward the electrocatalytic reduction of H_2O_2, while simultaneously having low catalytic activity in the decomposition of H_2O_2 into oxygen and water, thus they offer several possibilities for the construction of more effective biosensors and as the electroactive materials in fuel cells.

Notes

The authors declare no competing financial interests.

Acknowledgment

The authors thank the National Science Council, Poland, for their generous support of this work (grant: #2012/05/E/ST5/03800 to M.E.P.-B. and grant: OPUS 13 UMO – 2017/25/B/ST5/00975 to A.P.T.). L.E. thanks the Robert A. Welch Foundation for an endowed chair, grant #AH-0033 and the US NSF, grants: PREM program (DMR-1205302) and CHE-1801317. The XPS studies were carried out with the equipment purchased thanks to the financial support of the European Regional Development Fund (contract No. POIG.02.01.00-06024/09 - Centre of Functional Nanomaterials, Lublin, Poland).

Appendix A. Supplementary data

Supplementary data to this article can be found online at https://doi.org/10.1016/j.carbon.2019.05.069.

References

[1] O. Mykhailiv, H. Zubyk, K. Brzezinski, M. Gras, G. Lota, M. Gniadek, E. Romero, L. Echegoyen, M.E. Plonska-Brzezinska, Improvement of the structural and chemical properties of carbon nano-onions for electrocatalysis, ChemNanoMat 3 (2017) 583–590, https://doi.org/10.1002/cnma.201700161.
[2] V.L. Kuznetsov, Y.V. Butenko, Nanodiamond graphitization and properties of onion-like carbon, in: D.M. Gruen, O.A. Shenderova, A.Y. Vul' (Eds.), Synthesis, Properties and Applications of Ultrananocrystalline Diamond, Springer-Verlag, Berlin/Heidelberg, 2005, pp. 199–216. http://link.springer.com/10.1007/1-4020-3322-2_15. (Accessed 17 January 2015).
[3] V.L. Kuznetsov, Y.V. Butenko, Synthesis and properties of nanostructured carbon materials: nanodiamond, onion-like carbon and carbon nanotubes, in: Y.G. Gogotsi, I.V. Uvarova (Eds.), Nanostructured Materials and Coatings for Biomedical and Sensor Applications, Springer Netherlands, Dordrecht, 2003, pp. 187–202. http://link.springer.com/10.1007/978-94-010-0157-1_20. (Accessed 4 October 2016).
[4] V.L. Kuznetsov, A.L. Chuvilin, Y.V. Butenko, I.Y. Mal'kov, V.M. Titov, Onion-like carbon from ultra-disperse diamond, Chem. Phys. Lett. 222 (1994) 343–348, https://doi.org/10.1016/0009-2614(94)87072-1.
[5] R. Al-Jishi, G. Dresselhaus, Lattice-dynamical model for graphite, Phys. Rev. B 26 (1982) 4514–4522, https://doi.org/10.1103/PhysRevB.26.4514.
[6] A.E. Aleksenskii, M.V. Baidakova, A.Y. Vul, V.Y. Davydov, Y.A. Pevtsova, Diamond-graphite phase transition in ultradisperse-diamond clusters, Phys. Solid State 39 (1997) 1007–1015, https://doi.org/10.1134/1.1129989.
[7] H. Pinto, A. Markevich, Electronic and electrochemical doping of graphene by surface adsorbates, Beilstein J. Nanotechnol. 5 (2014) 1842–1848, https://doi.org/10.3762/bjnano.5.195.
[8] D. Kepaptsoglou, T.P. Hardcastle, C.R. Seabourne, U. Bangert, R. Zan, J.A. Amani, H. Hofsäss, R.J. Nicholls, R.M.D. Brydson, A.J. Scott, Q.M. Ramasse, Electronic structure modification of ion implanted graphene: the spectroscopic signatures of p- and n-type doping, ACS Nano 9 (2015) 11398–11407, https://doi.org/10.1021/acsnano.5b05305.
[9] S.S. Chauhan, P. Srivastava, A.K. Shrivastava, Electronic and transport properties of boron and nitrogen doped graphene nanoribbons: an ab initio approach, Appl. Nanosci. 4 (2014) 461–467, https://doi.org/10.1007/s13204-013-0220-2.
[10] G.A. Ferrero, K. Preuss, A. Marinovic, A.B. Jorge, N. Mansor, D.J.L. Brett, A.B. Fuertes, M. Sevilla, M.-M. Titirici, Fe–N-Doped carbon capsules with outstanding electrochemical performance and stability for the oxygen reduction reaction in both acid and alkaline conditions, ACS Nano 10 (2016) 5922–5932, https://doi.org/10.1021/acsnano.6b01247.
[11] M. Blanco, P. Álvarez, C. Blanco, M.V. Jiménez, J.J. Pérez-Torrente, L.A. Oro, J. Blasco, V. Cuartero, R. Menéndez, Enhancing the hydrogen transfer catalytic activity of hybrid carbon nanotube-based NHC–iridium catalysts by increasing the oxidation degree of the nanosupport, Catal. Sci. Technol. 6 (2016) 5504–5514, https://doi.org/10.1039/C5CY01998B.
[12] B. Nagy, S. Villar-Rodil, J.M.D. Tascón, I. Bakos, K. László, Nitrogen doped mesoporous carbon aerogels and implications for electrocatalytic oxygen reduction reactions, Microporous Mesoporous Mater. 230 (2016) 135–144, https://doi.org/10.1016/j.micromeso.2016.05.009.
[13] K.N. Wood, R. O'Hayre, S. Pylypenko, Recent progress on nitrogen/carbon structures designed for use in energy and sustainability applications, Energy Environ. Sci. 7 (2014) 1212, https://doi.org/10.1039/c3ee44078h.
[14] X. Bo, M. Zhou, L. Guo, Electrochemical sensors and biosensors based on less aggregated graphene, Biosens. Bioelectron. (2016), https://doi.org/10.1016/j.bios.2016.05.002.
[15] P. Wu, P. Du, H. Zhang, C. Cai, Microscopic effects of the bonding configuration of nitrogen-doped graphene on its reactivity toward hydrogen peroxide reduction reaction, Phys. Chem. Chem. Phys. 15 (2013) 6920, https://doi.org/10.1039/c3cp50900a.
[16] X. Xu, S. Jiang, Z. Hu, S. Liu, Nitrogen-doped carbon nanotubes: high electrocatalytic activity toward the oxidation of hydrogen peroxide and its application for biosensing, ACS Nano 4 (2010) 4292–4298, https://doi.org/10.1021/nn1010057.
[17] L.G. Bulusheva, A.V. Okotrub, A.G. Kurenya, H. Zhang, H. Zhang, X. Chen, H. Song, Electrochemical properties of nitrogen-doped carbon nanotube

anode in Li-ion batteries, Carbon 49 (2011) 4013–4023, https://doi.org/10.1016/j.carbon.2011.05.043.
[18] K. Gong, F. Du, Z. Xia, M. Durstock, L. Dai, Nitrogen-doped carbon nanotube Arrays with high electrocatalytic activity for oxygen reduction, Science 323 (2009) 760–764, https://doi.org/10.1126/science.1168049.
[19] J.M. Goran, E.N.H. Phan, C.A. Favela, K.J. Stevenson, H2O2 detection at carbon nanotubes and nitrogen-doped carbon nanotubes: oxidation, reduction, or disproportionation? Anal. Chem. 87 (2015) 5989–5996, https://doi.org/10.1021/acs.analchem.5b00059.
[20] J.C. Carrero-Sánchez, A.L. Elías, R. Mancilla, G. Arrellín, H. Terrones, J.P. Laclette, M. Terrones, Biocompatibility and toxicological studies of carbon nanotubes doped with nitrogen, Nano Lett. 6 (2006) 1609–1616, https://doi.org/10.1021/nl060548p.
[21] J.M. Goran, K.J. Stevenson, Electrochemical behavior of flavin adenine dinucleotide adsorbed onto carbon nanotube and nitrogen-doped carbon nanotube electrodes, Langmuir 29 (2013) 13605–13613, https://doi.org/10.1021/la403020y.
[22] J.D. Wiggins-Camacho, K.J. Stevenson, Effect of nitrogen concentration on capacitance, density of states, electronic conductivity, and morphology of N-doped carbon nanotube electrodes, J. Phys. Chem. C 113 (2009) 19082–19090, https://doi.org/10.1021/jp907160v.
[23] S.J. Amirfakhri, D. Binny, J.-L. Meunier, D. Berk, Investigation of hydrogen peroxide reduction reaction on graphene and nitrogen doped graphene nanoflakes in neutral solution, J. Power Sources 257 (2014) 356–363, https://doi.org/10.1016/j.jpowsour.2014.01.114.
[24] E. Kjeang, N. Djilali, D. Sinton, Microfluidic fuel cells: a review, J. Power Sources 186 (2009) 353–369, https://doi.org/10.1016/j.jpowsour.2008.10.011.
[25] J.-C. Shyu, C.-L. Huang, Characterization of bubble formation in microfluidic fuel cells employing hydrogen peroxide, J. Power Sources 196 (2011) 3233–3238, https://doi.org/10.1016/j.jpowsour.2010.12.005.
[26] K. Chatterjee, M. Ashokkumar, H. Gullapalli, Y. Gong, R. Vajtai, P. Thanikaivelan, P.M. Ajayan, Nitrogen-rich carbon nano-onions for oxygen reduction reaction, Carbon 130 (2018) 645–651, https://doi.org/10.1016/j.carbon.2018.01.052.
[27] A.S. Rettenbacher, B. Elliott, J.S. Hudson, A. Amirkhanian, L. Echegoyen, Preparation and functionalization of multilayer fullerenes (carbon nano-onions), Chem. Eur J. 12 (2006) 376–387, https://doi.org/10.1002/chem.200500517.
[28] P. Olejnik, M. Gniadek, L. Echegoyen, M. Plonska-Brzezinska, Nanoforest: polyaniline nanotubes modified with carbon nano-onions as a nanocomposite material for easy-to-miniaturize high-performance solid-state supercapacitors, Polymers 10 (2018) 1408, https://doi.org/10.3390/polym10121408.
[29] H. Falcón, R.E. Carbonio, Study of the heterogeneous decomposition of hydrogen peroxide: its application to the development of catalysts for carbon-based oxygen cathodes, J. Electroanal. Chem. 339 (1992) 69–83, https://doi.org/10.1016/0022-0728(92)80445-A.
[30] D. Wei, Y. Liu, Y. Wang, H. Zhang, L. Huang, G. Yu, Synthesis of N-doped graphene by chemical vapor deposition and its electrical properties, Nano Lett. 9 (2009) 1752–1758, https://doi.org/10.1021/nl803279t.
[31] A. Dimiev, D.V. Kosynkin, A. Sinitskii, A. Slesarev, Z. Sun, J.M. Tour, Layer-by-Layer removal of graphene for device patterning, Science 331 (2011) 1168–1172, https://doi.org/10.1126/science.1199183.
[32] O. Mykhailiv, K. Brzezinski, B. Sulikowski, Z. Olejniczak, M. Gras, G. Lota, A. Molina-Ontoria, M. Jakubczyk, L. Echegoyen, M.E. Plonska-Brzezinska, Boron-doped polygonal carbon nano-onions: synthesis and applications in electrochemical energy storage, Chem. Eur J. 23 (2017) 7132–7141, https://doi.org/10.1002/chem.201700914.
[33] T. Sharifi, F. Nitze, H.R. Barzegar, C.-W. Tai, M. Mazurkiewicz, A. Malolepszy, L. Stobinski, T. Wågberg, Nitrogen doped multi walled carbon nanotubes produced by CVD-correlating XPS and Raman spectroscopy for the study of nitrogen inclusion, Carbon 50 (2012) 3535–3541, https://doi.org/10.1016/j.carbon.2012.03.022.
[34] C. Morant, J. Andrey, P. Prieto, D. Mendiola, J.M. Sanz, E. Elizalde, XPS characterization of nitrogen-doped carbon nanotubes, Phys. Status Solidi 203 (2006) 1069–1075, https://doi.org/10.1002/pssa.200566110.
[35] T. Susi, T. Pichler, P. Ayala, X-ray photoelectron spectroscopy of graphitic carbon nanomaterials doped with heteroatoms, Beilstein J. Nanotechnol. 6 (2015) 177–192, https://doi.org/10.3762/bjnano.6.17.
[36] J.R. Pels, F. Kapteijn, J.A. Moulijn, Q. Zhu, K.M. Thomas, Evolution of nitrogen functionalities in carbonaceous materials during pyrolysis, Carbon 33 (1995) 1641–1653, https://doi.org/10.1016/0008-6223(95)00154-6.
[37] W. Shen, Z. Li, Y. Liu, Surface chemical functional groups modification of porous carbon, Recent Pat. Chem. Eng. 1 (2008) 27–40, https://doi.org/10.2174/2211334710801010027.
[38] V.R. Dhanak, YuV. Butenko, A.C. Brieva, P.R. Coxon, L. Alves, L. Šiller, Chemical functionalization of nanodiamond by amino groups: an X-ray photoelectron spectroscopy study, J. Nanosci. Nanotechnol. 12 (2012) 3084–3090, https://doi.org/10.1166/jnn.2012.4547.
[39] M.M. Dubinin, E.D. Zaverina, V.V. Serpinsky, The sorption of water vapour by active carbon, J. Chem. Soc. (1955) 1760, https://doi.org/10.1039/jr9550001760.
[40] M.M. Dubinin, A.A. Isirikyan, Heat of adsorption of water vapors on active carbons, Bulletin of the Academy of Sciences of the USSR Division of Chemical Science 38 (1989) 2002–2004, https://doi.org/10.1007/BF00962094.
[41] M.M. Dubinin, V. Serpinsky, Isotherm equation for water vapor adsorption by microporous carbonaceous adsorbents, Carbon 19 (1981) 402–403, https://doi.org/10.1016/0008-6223(81)90066-X.
[42] S. Furmaniak, P.A. Gauden, A.P. Terzyk, G. Rychlicki, Water adsorption on carbons — critical review of the most popular analytical approaches, Adv. Colloid Interface Sci. 137 (2008) 82–143, https://doi.org/10.1016/j.cis.2007.08.001.
[43] A.P. Terzyk, P.A. Gauden, G. Rychlicki, Energetics of water adsorption and immersion on carbons, Colloid. Surf. Physicochem. Eng. Asp. 148 (1999) 271–281, https://doi.org/10.1016/S0927-7757(98)00770-5.
[44] M. Polovina, B. Babić, B. Kaluderović, A. Dekanski, Surface characterization of oxidized activated carbon cloth, Carbon 35 (1997) 1047–1052, https://doi.org/10.1016/S0008-6223(97)00057-2.
[45] R.H. Bradley, I. Sutherland, E. Sheng, Relationship between carbon black surface chemistry and energy, J. Chem. Soc. Faraday. Trans. 91 (1995) 3201, https://doi.org/10.1039/ft9959103201.
[46] A.P. Terzyk, The influence of activated carbon surface chemical composition on the adsorption of acetaminophen (paracetamol) in vitro, Colloid. Surf. Physicochem. Eng. Asp. 177 (2001) 23–45, https://doi.org/10.1016/S0927-7757(00)00594-X.
[47] A. Toth, K.V. Voitko, Ol Bakalinska, G.P. Prykhodko, I. Bertotic, A. Martınez-Alonso, J.M.D. Tascon, V.M. Gunko, K. Laszlo, Morphology and adsorption properties of chemically modified MWCNT probed by nitrogen, n-propane and water vapor, Carbon 50 (2012) 577–585, https://doi.org/10.1016/j.carbon.2011.09.016.
[48] K.V. Voitko, R.L.D. Whitby, V.M. Gun'ko, O.M. Bakalinska, M.T. Kartel, K. Laszlo, A.B. Cundy, S.V. Mikhalovsky, Morphological and chemical features of nano and macroscale carbons affecting hydrogen peroxide decomposition in aqueous media, J. Colloid Interface Sci. 361 (2011) 129–136, https://doi.org/10.1016/j.jcis.2011.05.048.
[49] L.B. Khalil, B.S. Girgis, T.A. Tawfik, Decomposition of H_2O_2 on activated carbon obtained from olive stones, J. Chem. Technol. Biotechnol. 76 (2001) 1132–1140, https://doi.org/10.1002/jctb.481.
[50] A. Rey, J.A. Zazo, J.A. Casas, A. Bahamonde, J.J. Rodriguez, Influence of the structural and surface characteristics of activated carbon on the catalytic decomposition of hydrogen peroxide, Appl. Catal. Gen. 402 (2011) 146–155, https://doi.org/10.1016/j.apcata.2011.05.040.
[51] L.C. Oliveira, C.N. Silva, M.I. Yoshida, R.M. Lago, The effect of H2 treatment on the activity of activated carbon for the oxidation of organic contaminants in water and the H_2O_2 decomposition, Carbon 42 (2004) 2279–2284, https://doi.org/10.1016/j.carbon.2004.05.003.
[52] G. Fang, C. Liu, J. Gao, D. Zhou, New insights into the mechanism of the catalytic decomposition of hydrogen peroxide by activated carbon: implications for degradation of diethyl phthalate, Ind. Eng. Chem. Res. 53 (2014) 19925–19933, https://doi.org/10.1021/ie504184r.
[53] V.V. Strelko, Role of carbon matrix heteroatoms at synthesis of carbons for catalysis and energy applications, J. Energy Chem. 22 (2013) 174–182, https://doi.org/10.1016/S2095-4956(13)60023-6.
[54] V. Strelko, V. Kuts, P. Thrower, On the mechanism of possible influence of heteroatoms of nitrogen, boron and phosphorus in a carbon matrix on the catalytic activity of carbons in electron transfer reactions, Carbon 38 (2000) 1499–1503, https://doi.org/10.1016/S0008-6223(00)00121-4.
[55] E. Vega, H. Valdés, New evidence of the effect of the chemical structure of activated carbon on the activity to promote radical generation in an advanced oxidation process using hydrogen peroxide, Microporous Mesoporous Mater. 259 (2018) 1–8, https://doi.org/10.1016/j.micromeso.2017.09.018.
[56] R.S. Ribeiro, A.M.T. Silva, J.L. Figueiredo, J.L. Faria, H.T. Gomes, The influence of structure and surface chemistry of carbon materials on the decomposition of hydrogen peroxide, Carbon 62 (2013) 97–108, 1016/j.carbon.2013.06.13.
[57] B. Weng, A. Morrin, R. Shepherd, K. Crowley, A.J. Killard, P.C. Innis, G.G. Wallace, Wholly printed polypyrrole nanoparticle-based biosensors on flexible substrate, J. Mater. Chem. B. 2 (2014) 793–799, https://doi.org/10.1039/C3TB21378A.
[58] E. Ferapontova, E. Puganova, Effect of pH on direct electron transfer between graphite and horseradish peroxidase, J. Electroanal. Chem. 518 (2002) 20–26, https://doi.org/10.1016/S0022-0728(01)00692-1.
[59] G. Lenaz (Ed.), Bioelectrochemistry of Biomacromolecules, Birkhäuser, Basel, 1997.
[60] Y. Yang, M. Yang, H. Wang, J. Jiang, G. Shen, R. Yu, An amperometric horseradish peroxidase inhibition biosensor based on a cysteamine self-assembled monolayer for the determination of sulfides, Sensor. Actuator. B Chem. 102 (2004) 162–168, https://doi.org/10.1016/j.snb.2004.04.016.
[61] Y. Zhang, J. Zhang, X. Huang, X. Zhou, H. Wu, S. Guo, Assembly of graphene oxide-enzyme conjugates through hydrophobic interaction, Small 8 (2012) 154–159, https://doi.org/10.1002/smll.201101695.
[62] Z. Xiaoyan, J. Yuanyuan, L. Zaijun, G. Zhiguo, W. Guangli, Improved activity and thermo-stability of the horse radish peroxidase with graphene quantum dots and its application in fluorometric detection of hydrogen peroxide, Spectrochim. Acta Mol. Biomol. Spectrosc. 165 (2016) 106–113, https://doi.org/10.1016/j.saa.2016.03.049.
[63] V.L. Kuznetsov, Y.V. Butenko, A.L. Chuvilin, A.I. Romanenko, A.V. Okotrub, Electrical resistivity of graphitized ultra-disperse diamond and onion-like carbon, Chem. Phys. Lett. 336 (2001) 397–404, https://doi.org/10.1016/S0009-2614(01)00135-X.
[64] J.K. McDonough, A.I. Frolov, V. Presser, J. Niu, C.H. Miller, T. Ubieto, M.V. Fedorov, Y. Gogotsi, Influence of the structure of carbon onions on their electrochemical performance in supercapacitor electrodes, Carbon 50 (2012) 3298–3309, https://doi.org/10.1016/j.carbon.2011.12.022.